Available online at www.sciencedirect.com
SCIENCE DIRECT®
ELSEVIER
Journal of Magnetism and Magnetic Materials 285 (2005) L1–L10
Journal of magnetism and magnetic materials
www.elsevier.com/locate/jmmm

Letter to the Editor

General magnetostatic shape–shape interactions

M. Beleggia[a], M. De Graef[b,*]

[a]Center for Functional Nanomaterials, Brookhaven National Laboratory, Upton, NY 11973, USA
[b]Department of Materials Science and Engineering, Carnegie Mellon University, 5000 Forbes Avenue, Pittsburgh, PA 15213-3890, USA

Received 16 July 2004; received in revised form 1 September 2004
Available online 1 October 2004

Abstract

The magnetostatic interaction energy between two magnetic elements of arbitrary shape is presented as a convolution between the cross-correlation of the particle shapes and the dipolar tensor field. A generalized dipole–dipole interaction is derived, where the magnetic moments associated with the two particles interact through a magnetometric tensor field, carrying all the shape information. Example computations are given in order to verify the correctness of the formalism. The well-known result of the interaction between prisms, employed in most micromagnetic simulations, is correctly retrieved. The numerical accuracy of the method is also compared to a simple analytical result. Finally, one additional example computation, two interlaced interacting rings, is presented to show the generality of the formalism.

PACS: 41.20.Gz; 75.30.Gw; 75.40.Mg; 75.75.+a

Keywords: Magnetostatic energy; Shape amplitude; Magnetic nanoparticles

1. Introduction

The calculation of the magnetostatic interaction energy, E_m, between multiple uniformly magnetized particles of arbitrary shape represents one of the most difficult components of a typical micromagnetic computation. In fact, it requires the evaluation of a six-fold integral for each pair of magnetic elements, as each magnetic moment of the first element interacts with each moment of the second (a first three-fold integration), and then all the moments of the first particle must be considered (another three-fold integration). This must then be repeated for each pair of magnetic elements. For a review of the literature on the topic of magnetostatic energy computations we refer to Chapters 7 and 11 in Ref. [1]. The six-fold integrations can be avoided in principle, by reformulating the equations of micromagnetics in terms of field Lagrangians [2], but this approach is not commonly used in contemporary micromagnetics software.

*Corresponding author. Tel.: +1 412 268 8527; fax: +1 412 268 7596.
E-mail address: degraef@cmu.edu (M. De Graef).

0304-8853/$ - see front matter © 2004 Elsevier B.V. All rights reserved.
doi:10.1016/j.jmmm.2004.09.004

Many micromagnetic simulation packages use rectangular prisms to subdivide the volume of a magnetic shape, and then employ pre-calculated coefficients, based on the functions first derived by Rhodes and Rowlands [3], to compute the pairwise interactions between all prisms. When a different shape is needed for the computations, then these coefficients must be recomputed. For most shapes, the integrals involved can not be solved analytically, so that numerical computations must be used. Simulations of blocking effects and magnetostatic interactions in random particle arrays (i.e., particles not arranged on a periodic lattice) are often carried out by truncating the long-range interactions at an appropriate radius [4]. Ewald summation schemes are also frequently used [5]. In dilute dispersions of single domain Fe particles in an insulating matrix, magnetostatic interactions were shown to be dominant even at packing fractions as low as 10% [5]. In such studies, the actual particle shapes are not taken into account, and all particles are assumed to behave as point dipoles [6], an assumption that has been shown to be inaccurate for small particle separations when the actual particle shape is properly taken into account [7]. Magnetostatic interactions can also be computed indirectly by considering the demagnetizing field; in such an approach, the demagnetizing field at a point in space due to a magnetized object is computed by dividing this object into small (cubic) cells, and then summing over all cells. This procedure is then repeated for all cells in a second body, so that the interaction energy can be computed [8].

It is the purpose of this Letter to introduce a novel theoretical and computational approach which reformulates the magnetostatic interaction energy as a convolution product between a function determined by the shape of the individual particles, and the dipolar interaction tensor field. The approach is very general, and permits evaluation (mostly numerical, but in some cases also analytical) of the shape–shape pair interaction energy. We begin this Letter with an explicit derivation of the new formalism, followed by a series of example computations. We conclude with the outline of a numerical algorithm for the computation of the magnetostatic interaction energy, with a final explicit example: two interlaced magnetized rings.

2. Theoretical model

The theoretical approach employs the concept of the *characteristic function* or *shape function*, $D(\mathbf{r})$, which is a discontinuous function equal to unity inside the particle and zero outside. For a particle with a uniform magnetization state, the magnetization can be expressed as a vector field $\mathbf{M}(\mathbf{r}) = M_0\hat{\mathbf{m}}D(\mathbf{r})$, where M_0 is the saturation magnetization and a hat indicates a unit vector. It was shown in Ref. [9], that the Fourier transform of the shape function, the so-called *shape amplitude* $D(\mathbf{k})$, is a continuous function that can be used to define the demagnetization tensor field $N^{\alpha\beta}(\mathbf{k}) = D(\mathbf{k})\hat{k}^{\alpha}\hat{k}^{\beta}$. We denote vector and tensor components with Greek superscripts. $\hat{k}^{\alpha} = k^{\alpha}/|\mathbf{k}|$ is the direction cosine of the α component of $\mathbf{k}$. The real space representation, $N^{\alpha\beta}(\mathbf{r})$, can be obtained by a three-dimensional (3D) inverse Fourier transformation. The shape amplitude is hence central to the description of the magnetostatic behavior of a uniformly magnetized particle.

It was also shown, in Ref. [7], that the demagnetization tensor field can be written as the convolution between the shape function and the dipolar tensor, $D^{\alpha\beta}(\mathbf{r})$

$$N^{\alpha\beta}(\mathbf{r}) = D(\mathbf{r}) \otimes \mathscr{F}^{-1}[\hat{k}^{\alpha}\hat{k}^{\beta}] = D(\mathbf{r}) \otimes \mathscr{D}^{\alpha\beta}(\mathbf{r}), \qquad (1)$$

where $\otimes$ represents the convolution product, and $\mathscr{F}$ the Fourier transform operator. The dipolar tensor is defined as

$$\mathscr{D}^{\alpha\beta}(\mathbf{r}) \equiv \frac{1}{4\pi r^5}[r^2\delta^{\alpha\beta} - 3r^{\alpha}r^{\beta}], \qquad (2)$$

where $r = |\mathbf{r}|$, and $\delta^{\alpha\beta}$ is the identity matrix. Examples of the computation of the demagnetization tensor field using this approach were described in Refs. [10,11].

Once the demagnetization tensor field (DTF) is known, then the magnetostatic energy can be computed by contracting the tensor with respect to the magnetization unit vector, $m^{\alpha}N^{\alpha\beta}(\mathbf{r})m^{\beta}$ (a summation over repeated superscripts is implied), and integrating over the complete volume of the

particle. Since the DTF was defined in terms of the dipolar tensor and the shape function, one could suspect that there must be a similar way to express the magnetostatic energy in terms of the same quantities. In the following paragraphs we will show how this can be accomplished.

It has been shown in Refs. [7,12] that the most general expression for the magnetostatic energy E_m of a magnetic system can be written as

$$E_\mathrm{m} = \frac{\mu_0}{16\pi^3}\int \frac{\mathrm{d}^3\mathbf{k}}{k^2}\,|\,\mathbf{M}(\mathbf{k})\cdot\mathbf{k}\,|^2. \tag{3}$$

If the magnetic system is a pair of uniformly magnetized particles, each of them described by a shape function $D_i(\mathbf{r})$ $(i=1,2)$, a magnetization saturation M_i, and a unit vector $\hat{\mathbf{m}}_i$, we can express the interaction part of Eq. (3) as

$$E_\mathrm{m} = \frac{\bar{K}_d}{4\pi^3}\,\Re\left[\int \mathrm{d}^3\mathbf{k}\, D_1(\mathbf{k})D_2^*(\mathbf{k}) \times(\hat{\mathbf{m}}_1\cdot\hat{\mathbf{k}})(\hat{\mathbf{m}}_2\cdot\hat{\mathbf{k}})\mathrm{e}^{\mathrm{i}\mathbf{k}\cdot\boldsymbol{\rho}}\right], \tag{4}$$

where $\boldsymbol{\rho}\equiv\mathbf{R}_1-\mathbf{R}_2$ is the relative position of the two particles.

In this expression, $\Re$ indicates the real part, and the mean magnetostatic energy density is defined as $\bar{K}_d\equiv\frac{1}{2}\mu_0 M_1 M_2=\sqrt{K_{d,1}K_{d,2}}$ with $K_{d,i}=\frac{1}{2}\mu_0 M_i^2$. The integral in this expression is an inverse Fourier transform with respect to the relative position vector $\boldsymbol{\rho}$, so we find

$$E_\mathrm{m} = 2\bar{K}_d m_1^\alpha m_2^\beta \Re\left\{\mathscr{F}_{\boldsymbol{\rho}}^{-1}\left[D_1(\mathbf{k})D_2^*(\mathbf{k})\hat{k}^\alpha\hat{k}^\beta\right]\right\} \tag{5}$$

From here on we will drop the $\Re$ symbol, since it is clear that the energy must always be a real number. Using the convolution theorem and Eq. (1), we have

$$\begin{aligned}\mathscr{F}_{\boldsymbol{\rho}}^{-1}&[D_1(\mathbf{k})D_2^*(\mathbf{k})\hat{k}^\alpha\hat{k}^\beta]\\ &=\mathscr{F}_{\boldsymbol{\rho}}^{-1}[D_1(\mathbf{k})D_2^*(\mathbf{k})]\otimes\mathscr{F}_{\boldsymbol{\rho}}^{-1}[k^\alpha k^\beta]\\ &=\mathscr{C}(\boldsymbol{\rho})\otimes\mathscr{D}^{\alpha\beta}(\boldsymbol{\rho}).\end{aligned} \tag{6}$$

In this expression we have introduced the function $\mathscr{C}(\mathbf{r})$, which is defined as the cross-correlation of the two shape functions: $\mathscr{C}(\mathbf{r})=D_1(\mathbf{r})\otimes D_2(-\mathbf{r})\equiv D_1(\mathbf{r})\star D_2(\mathbf{r})$, where we follow Bracewell [13] in denoting the cross-correlation by a $\star$ (pentagram).

Combining all equations, we find as the final expression for the magnetostatic interaction energy

$$E_\mathrm{m}(\boldsymbol{\rho};\hat{\mathbf{m}}_1,\hat{\mathbf{m}}_2) = 2\bar{K}_d\, m_1^\alpha[\mathscr{C}(\boldsymbol{\rho})\otimes\mathscr{D}^{\alpha\beta}(\boldsymbol{\rho})]m_2^\beta. \tag{7}$$

It is easy to show that this expression reduces to the more familiar dipolar interaction energy in the limit that individual particles become single magnetic dipoles. The shape function for a point dipole is the weighted Dirac delta function, $V\delta(\mathbf{r})$, so that $\mathscr{C}(\mathbf{r})=V^2\delta(\mathbf{r})\otimes\delta(\mathbf{r})=V^2\delta(\mathbf{r})$, where we have used the fact that $\delta(\mathbf{r})$ is the identity function for the convolution product. Substitution in Eq. (7) results in the standard dipolar energy expression

$$\begin{aligned}E_\mathrm{m}(\boldsymbol{\rho}) &= 2\bar{K}_d V^2\, m_1^\alpha\mathscr{D}^{\alpha\beta}(\boldsymbol{\rho})m_2^\beta\\ &=\mu_0\boldsymbol{\mu}_1:\mathscr{D}(\boldsymbol{\rho}):\boldsymbol{\mu}_2\\ &=\frac{\mu_0}{4\pi}\left[\frac{\boldsymbol{\mu}_1\cdot\boldsymbol{\mu}_2}{\rho^3}-3\frac{(\boldsymbol{\mu}_1\cdot\boldsymbol{\rho})(\boldsymbol{\mu}_2\cdot\boldsymbol{\rho})}{\rho^5}\right]\end{aligned} \tag{8}$$

with the standard definition of the magnetic moments $\boldsymbol{\mu}_i=M_i\hat{\mathbf{m}}_i V$, and denoting as : the tensor contraction operation.

If we now define the tensor field

$$\mathscr{N}^{\alpha\beta}(\boldsymbol{\rho}) = \frac{1}{V_1 V_2}\,\mathscr{C}(\boldsymbol{\rho})\otimes\mathscr{D}^{\alpha\beta}(\boldsymbol{\rho}) \tag{9}$$

then the interaction energy can be written as

$$\begin{aligned}E_\mathrm{m}(\boldsymbol{\rho};\hat{\mathbf{m}}_1,\hat{\mathbf{m}}_2) &= 2\bar{K}_d V_1 V_2\, m_1^\alpha\mathscr{N}^{\alpha\beta}(\boldsymbol{\rho})m_2^\beta\\ &=\mu_0\,\boldsymbol{\mu}_1:\mathscr{N}(\boldsymbol{\rho}):\boldsymbol{\mu}_2,\end{aligned} \tag{10}$$

which is strikingly similar to Eq. (8). We have thus derived a generalized dipole–dipole interaction, where instead of each single elementary magnetic moment (spin) of particle 1 interacting with each other spin of particle 2 through the simple dipolar tensor, the whole magnetic moment associated to particle 1 interacts with the whole magnetic moment associated to particle 2 through a less simple tensor, which includes all the shape-related information. The advantage of the present formalism is dramatic: while the spin pair interaction is then to be repeated and summed over each couple of spins, with Eq. (10) the calculation is to be done only once.

It is interesting to consider the relation between the new tensor field $\mathscr{N}^{\alpha\beta}(\boldsymbol{\rho})$ and the magnetometric

(volume averaged) demagnetization factors. It has been shown in Ref. [9] that the magnetometric demagnetization factors can be expressed as

$$\langle N\rangle^{\alpha\beta} = \frac{1}{8\pi^3 V}\int \mathrm{d}^3\mathbf{k}|D(\mathbf{k})|^2\hat{k}^\alpha\hat{k}^\beta \tag{11}$$

while for particles with identical shape, Eq. (9) can be written as

$$\mathscr{N}^{\alpha\beta}(\boldsymbol{\rho}) = \frac{1}{8\pi^3 V^2}\int \mathrm{d}^3\mathbf{k}|D(\mathbf{k})|^2\hat{k}^\alpha\hat{k}^\beta \mathrm{e}^{\mathrm{i}\mathbf{k}\cdot\boldsymbol{\rho}}. \tag{12}$$

It is then easy to see by comparing Eqs. (11) and (12) that for particles with identical shape $V\mathscr{N}^{\alpha\beta}(\mathbf{0}) = \langle N\rangle^{\alpha\beta}$. Because of this relation, we propose to call $\mathscr{N}^{\alpha\beta}(\boldsymbol{\rho})$ the *magnetometric tensor field*. It is easy to verify that the trace of $\mathscr{N}$ is equal to the trace of $\mathscr{D}$ and vanishes for non-overlapping particles.

3. Example applications

Before we consider an example application of the formalism, it is useful to recall briefly the geometrical meaning of the cross-correlation function: $\mathscr{C}(\boldsymbol{\rho})$ describes the volume that is common to the two shapes, when they (partially or completely) overlap, as a function of the relative position $\boldsymbol{\rho}$ of the two shapes. Note that for non-centrosymmetric shapes, a coordinate inversion must be carried out before computation of the cross- or auto-correlation. For simplicity, we will only consider identical shapes in the remainder of this section.

The auto-correlation function $\mathscr{C}(\boldsymbol{\rho})$ for three basic shapes, prism, sphere and cylinder, computed as $\mathscr{F}_{\boldsymbol{\rho}}^{-1}[|D(\mathbf{k})|^2]$, can be expressed as

$$\mathscr{C}(\rho_x,\rho_y,\rho_z) = (2a-|\rho_x|)(2b-|\rho_y|)(2c-|\rho_z|) \tag{13}$$

for a prism of sides $(2a, 2b, 2c)$ in cartesian coordinates and for $|\rho_x|<2a, |\rho_y|<2b, |\rho_z|<2c$;

$$\mathscr{C}(\rho,\rho_z) = \frac{2V}{\pi}\left(1-\frac{|\rho_z|}{t}\right) \times\left[\arccos\left(\frac{\rho}{2R}\right)-\frac{\rho}{2R}\sqrt{1-\left(\frac{\rho}{2R}\right)^2}\right] \tag{14}$$

for a cylinder of height t and radius R in a polar (ρ,ρ_z) coordinate system and for $|\rho_z|<t$, $0<\rho<2R$;

$$\mathscr{C}(\rho) = \frac{V}{16}\left(\frac{\rho}{R}-2\right)^2\left(\frac{\rho}{R}+4\right) \tag{15}$$

for a sphere of radius R in a spherical coordinate system and for $0<\rho<2$. All of the above functions are zero outside the specified region.

To show in more detail how the energy is computed in this approach, let us consider two cylinders with vertical magnetization, displaced at a distance ρ along the x-axis as sketched in Fig. 1. The convolution product in Eq. (7) can be written more explicitly as

$$E(\boldsymbol{\rho};\hat{\mathbf{m}}_1,\hat{\mathbf{m}}_2) = 2\bar{K}_d m_1^\alpha m_2^\beta\int \mathrm{d}^3\mathbf{r}\,\mathscr{C}(\mathbf{r})\mathscr{D}^{\alpha\beta}(\boldsymbol{\rho}-\mathbf{r}). \tag{16}$$

Since the cylinders are axially magnetized, as indicated by the arrows, the only component of the dipolar tensor that contributes to the

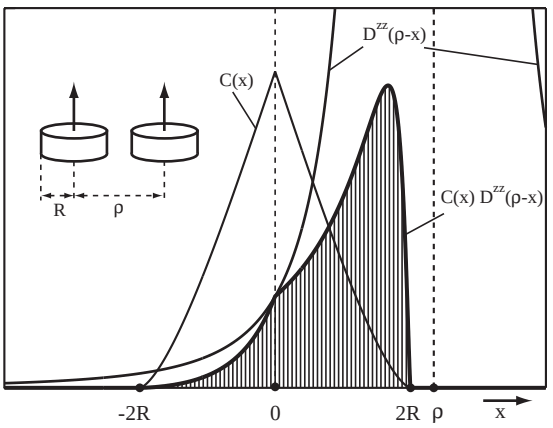

Fig. 1. 1D schematic illustration of the convolution process of Eq. (16) for two uniformly magnetized interacting cylinders (axial magnetization direction). The curve labeled $\mathscr{C}(x)$ represents the auto-correlation function of a cylinder with radius R. When the cylinders are located at a distance ρ along the x-axis, then the $D^{zz}(\rho-x)$ component of the dipolar tensor is centered at $\rho = x$. The product of the two functions is shown as a thick line, and is only non-zero in the range $-2R\leqslant x\leqslant 2R$. The area under the curve represents the contribution to the magnetostatic energy.

magnetostatic energy is

$$D^{zz}(\rho - x) = \frac{1}{4\pi|\rho - x|^3}. \tag{17}$$

This function is shown in the figure, together with the auto-correlation $\mathscr{C}(x)$ evaluated from Eq. (14). The dipolar component $D^{zz}(\rho - x)$ is centered around the position $\rho = x$. The product of the two functions, $\mathscr{C}(x)D^{zz}(\rho - x)$, is shown as a thicker line. The area under this curve represents the contribution to the total magnetostatic energy. This is obviously a simplified 1D case. In reality, the magnetostatic energy is the integral of the product of two 3D functions over the volume of the auto-correlation function. The divergence of the dipolar tensor component $D^{zz}(\rho - x)$ for $\rho = x$ does not represent a problem, since the point $\rho = x$ can never enter inside the range $-2R \leqslant x \leqslant 2R$ as the cylinders cannot physically overlap.

It is interesting to note that the expression for the magnetostatic energy in Eq. (16) represents a three-fold integration over a finite volume, namely the volume where the auto-correlation function is non-zero. The standard expression for the magnetostatic interaction energy of two interacting particles, which requires a six-fold integration over the two particle shapes, has been replaced by six three-fold integrations over the volume of the auto-correlation function, or, in the case of particles with different shapes, over the volume of the cross-correlation function. There are six integrations, one for each of the components of the symmetric dipolar tensor. This represents a significant simplification of the magnetostatic energy problem, since the numerical computation of $\mathscr{C}(\mathbf{r})$ is effortless.

Let us now consider a simple example where we can carry out the convolution in Eq. (16) explicitly: two interacting uniformly magnetized spheres of radius R located at a distance ρ along the z-axis (i.e., $\boldsymbol{\rho} = (0, 0, \rho)$). If the magnetizations of both spheres are perpendicular to their separation, for instance along the x-axis (i.e., $\hat{\mathbf{m}}_i = [1, 0, 0]$), then only one term survives in the tensor contraction of Eq. (16):

$$D^{xx}(\boldsymbol{\rho} - \mathbf{r}) = \frac{1}{4\pi} \frac{x^2 + y^2 + (\rho - z)^2 - 3x^2}{[x^2 + y^2 + (\rho - z)^2]^{5/2}}. \tag{18}$$

The simple geometry allows for a direct integration of Eq. (16) in spherical coordinates

$$E(\rho) = \frac{\bar{K}_d}{2\pi} \int_0^\infty r^2 \, \mathrm{d}r \, \mathscr{C}(r) \int_{-1}^{1} \mathrm{d}\xi \int_0^{2\pi} \mathrm{d}\phi \times \left[\frac{1}{(r^2 + \rho^2 - 2r\rho\xi)^{3/2}} - \frac{3r^2(1 - \xi^2)\cos^2\phi}{(r^2 + \rho^2 - 2r\rho\xi)^{5/2}} \right], \tag{19}$$

where $\mathscr{C}(r)$ is given in Eq. (15). The result is, as expected

$$E(\rho) = \frac{8\pi K_d R^6}{9\rho^3} = \frac{K_d V^2}{2\pi\rho^3} = \frac{\mu_0}{4\pi} \frac{\boldsymbol{\mu}_1 \cdot \boldsymbol{\mu}_2}{\rho^3} \tag{20}$$

coincident with the energy of two dipoles with magnetic moments $|\boldsymbol{\mu}_i| = M_i V$. It can also be verified, by direct computation, that for non-overlapping spheres (when $\rho > 2R$) the identity $\mathscr{N}^{\alpha\beta}(\boldsymbol{\rho}) = \mathscr{D}^{\alpha\beta}(\boldsymbol{\rho})$ holds: the magnetometric tensor field for two interacting spheres is the dipolar tensor itself. The situation is strikingly similar to the identity between the demagnetizing field of a uniformly magnetized sphere and the dipole field, valid in the region outside the sphere.

As a final analytical example, we consider now the interaction between magnetized prisms. This problem is fundamental in micromagnetics, and the method presented here must reproduce correctly the known and widely employed results. Considering two identical cubes with edge length $2a$ displaced by a vector $\boldsymbol{\rho} = [\rho_x, \rho_y, \rho_z]$, we have for the tensor element $\mathscr{N}^{zz}(\bar{\boldsymbol{\rho}})$:

$$\mathscr{N}^{zz}(\bar{\boldsymbol{\rho}}) = \frac{1}{32\pi a^3} \int_{-1}^{+1} \mathrm{d}\bar{x} \int_{-1}^{+1} \mathrm{d}\bar{y} \int_{-1}^{+1} \mathrm{d}\bar{z} \times (1 - |\bar{x}|)(1 - |\bar{y}|)(1 - |\bar{z}|) \times \frac{(\bar{\rho}_x - \bar{x})^2 + (\bar{\rho}_y - \bar{y})^2 - 2(\bar{\rho}_z - \bar{z})^2}{[(\bar{\rho}_x - \bar{x})^2 + (\bar{\rho}_y - \bar{y})^2 + (\bar{\rho}_z - \bar{z})^2]^{5/2}}, \tag{21}$$

where we have rescaled all distances by the cube edge length ($\bar{\mathbf{r}} = \mathbf{r}/2a$, $\bar{\boldsymbol{\rho}} = \boldsymbol{\rho}/2a$). Analytical computation of this three-fold integral is lengthy but

not difficult and results in

$$\begin{aligned}\mathcal{N}^{zz}(\bar{\boldsymbol{\rho}}) = \frac{1}{32\pi a^3}[&4H(\bar{\rho}_x,\bar{\rho}_y,\bar{\rho}_z)\\ &+H(\bar{\rho}_x,-1+\bar{\rho}_y,-1+\bar{\rho}_z)\\ &-2H(\bar{\rho}_x,\bar{\rho}_y,-1+\bar{\rho}_z)\\ &+H(\bar{\rho}_x,1+\bar{\rho}_y,-1+\bar{\rho}_z)\\ &+H(\bar{\rho}_x,-1+\bar{\rho}_y,1+\bar{\rho}_z)\\ &-2H(\bar{\rho}_x,\bar{\rho}_y,1+\bar{\rho}_z)\\ &+H(\bar{\rho}_x,1+\bar{\rho}_y,1+\bar{\rho}_z)\\ &-2H(\bar{\rho}_x,-1+\bar{\rho}_y,\bar{\rho}_z)\\ &-2H(\bar{\rho}_x,1+\bar{\rho}_y,\bar{\rho}_z)],\end{aligned} \tag{22}$$

where

$$\begin{aligned}H(x,y,z) \equiv\ & K(1+x,y,z)-2K(x,y,z)\\ &+K(-1+x,y,z)\end{aligned} \tag{23}$$

and, with $r=\sqrt{x^2+y^2+z^2}$

$$\begin{aligned}K(x,y,z) \equiv\ & \frac{r}{6}(r^2-3z^2)\\ &+xyz\,\arctan\left(\frac{xy}{zr}\right)-xy^2\,\ln(x+r)\\ &+\frac{x}{2}(y^2+z^2)\mathrm{arcsinh}\left(\frac{x}{\sqrt{y^2+z^2}}\right)\\ &+\frac{y}{2}(z^2-x^2)\mathrm{arcsinh}\left(\frac{y}{\sqrt{x^2+z^2}}\right).\end{aligned} \tag{24}$$

Special cases, when one or more of the components of $\bar{\boldsymbol{\rho}}$ vanishes, are readily derived from these relations by considering the appropriate limits in the inverse trigonometric and hyperbolic functions. The explicit expression for the tensor element $\mathcal{N}^{zz}(\bar{\boldsymbol{\rho}})$ consists of 135 terms. The other two diagonal tensor elements can be determined by an appropriate permutation of the coordinates, while for the off-diagonal elements of the tensor another explicit integration similar to Eq. (21) has to be computed. Detailed and accurate comparisons show that these results are in complete agreement with the well-known expressions for interacting prisms, used in most micromagnetics codes (e.g. Refs. [3,14,15]).

4. Numerical approach

Numerical implementation of the expressions derived in Section 2 can be done in two different ways. If the cross-correlation function of the particle shapes can be computed analytically (Section 3 lists a few of these functions for common simple shapes), then one could straightforwardly use a numerical integration scheme to compute the integrals for the tensor elements $\mathcal{N}^{\alpha\beta}(\boldsymbol{\rho})$.

Alternatively, if the particle shapes are too complex for analytical computation of the cross-correlation function, then the entire computation could be performed in Fourier space, as follows:

- Define the shape functions $D_i(\mathbf{r})$ of the particles on a discrete grid of N^3 points; grid points inside the particle are assigned a value of 1, others are set to zero;
- Use a fast Fourier transform (FFT) routine to compute the two shape amplitudes;
- Compute the 6 arrays $\hat{k}^{\alpha}\hat{k}^{\beta}$ (only 2 need to be stored; the others can be obtained by index permutations);
- Use the inverse FFT to compute the 6 components of the symmetric tensor field $\mathcal{N}^{\alpha\beta}$ for each particle pair, using the expression

$$\mathcal{N}^{\alpha\beta}(\boldsymbol{\rho}) = \frac{1}{V_1 V_2}\mathscr{F}_{\boldsymbol{\rho}}^{-1}[D_1(\mathbf{k})D_2^{*}(\mathbf{k})\hat{k}^{\alpha}\hat{k}^{\beta}]; \tag{25}$$

- Once the tensor fields are known, the magnetostatic energy of interacting particles can be computed using Eq. (10).

As a test to evaluate the accuracy of the proposed scheme, we consider again the same two spheres of radius R analyzed in Section 3. Calling now their displacement $\rho = 2R + d$, from Eq. (20) we obtain directly the relevant magnetometric tensor component $\mathcal{N}^{zz}(\rho)$:

$$\mathcal{N}^{zz}(\rho) = \frac{1}{4\pi(2R+d)^3} \tag{26}$$

and from Eq. (10) the interaction energy

$$E(\rho) = 2\bar{K}_d V^2 \mathcal{N}^{zz}(\rho)$$
$$= \bar{K}_d V^{zz}_{\text{eff}} \quad \text{with } V^{zz}_{\text{eff}} = \frac{8\pi R^6}{9(2R+d)^3}. \qquad (27)$$

V^{zz}_{eff} is the effective volume to be multiplied with the magnetostatic energy density to obtain the magnetostatic interaction energy.

The effective volume factor is shown as a continuous line in Fig. 2 for two spheres of radius $R = 10\,\text{nm}$, at a distance $(20 + d)\,\text{nm}$ from each other. The filled circles represent the results from a numerical simulation, using the method described earlier in this section. The effective volume factor is computed numerically from Eq. (25). The shape amplitudes were computed on a cubic grid of 256^3 nodes, with a grid spacing of 1 nm. The numerical results are in agreement with the theoretical expression, with a relative error of less than 1%.

As a second example, consider the magnetostatic interaction energy for a pair of interlaced uniformly magnetized rings with rectangular cross section, rotated with respect to each other as shown schematically in Fig. 3. The shape amplitude $D(\mathbf{k})$ for such a ring can be expressed analytically as

$$D(\mathbf{k}) = \frac{4\pi}{kk_z}[R_2 J_1(kR_2) - R_1 J_1(kR_1)]\sin(\mathrm{d}k_z), \qquad (28)$$

where $J_1(x)$ is the Bessel function of the first kind and first order, and (k, k_z) are the cylindrical components of the Fourier space frequency vector $\mathbf{k}$. Simulations were carried out on the same 256^3 pixels grid, with $R_1 = 10\,\text{nm}$, $R_2 = 15\,\text{nm}$, and $t = 2d = 4\,\text{nm}$.

The grayscale plots in Fig. 4(a) show the diagonal effective volume factors $V^{\alpha\alpha}_{\text{eff}}(x, y, 0)$. The off-diagonal elements vanish in this plane $z = 0$. The figure-eight shape visible in all images corresponds to position vectors $\boldsymbol{\rho}$ for which the two rings overlap; the tensor elements are put equal to zero in all such points. The grayscale ranges from $-45\,\text{nm}^3$ (black) to $+24\,\text{nm}^3$ (white).

Fig. 4(b) shows the effective volume factors in the plane $(x, y, 32)\,\text{nm}$, which corresponds to the case where the center of the ring with axis along the x-direction is located in the plane $z = 32\,\text{nm}$. There is then no overlap possible between the shapes, so that the effective volume factors are defined for all points (x, y). All six tensor elements are now different from zero, and the grayscale ranges from $-18\,\text{nm}^3$ (black) to $+9\,\text{nm}^3$ (white).

Fig. 5 shows the diagonal effective volume factors $V^{\alpha\alpha}_{\text{eff}}$ along the y-direction (a) and the

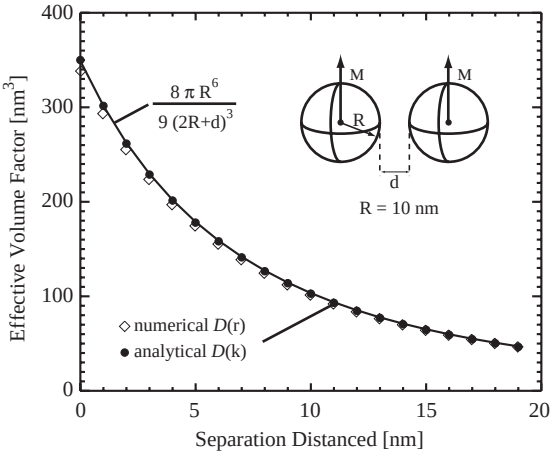

Fig. 2. Comparison of the effective volume factor for two interacting spheres with uniform magnetization along the z-direction. The spheres have a radius of 10 nm, and are separated by a distance ρ. The solid curve represents the analytical result, whereas the symbols indicate numerical results using Eq. (25). Solid circles were obtained starting from the Fourier space expression for the shape amplitude $D(\mathbf{k})$, whereas open diamonds were obtained starting from the real space shape function $D(\mathbf{r})$.

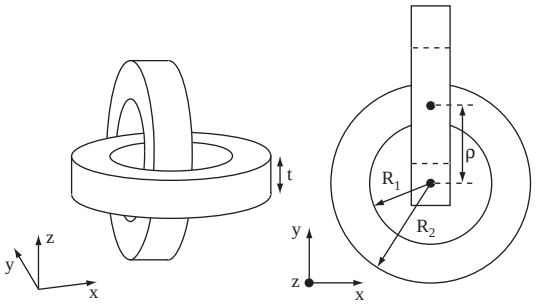

Fig. 3. Schematic illustration of two identical rings with inner radius R_1, outer radius R_2, and thickness t. The first ring is centered in the origin, whereas the center of the second ring is located at the point $[0, \frac{1}{2}(R_1 + R_2), 0]$.

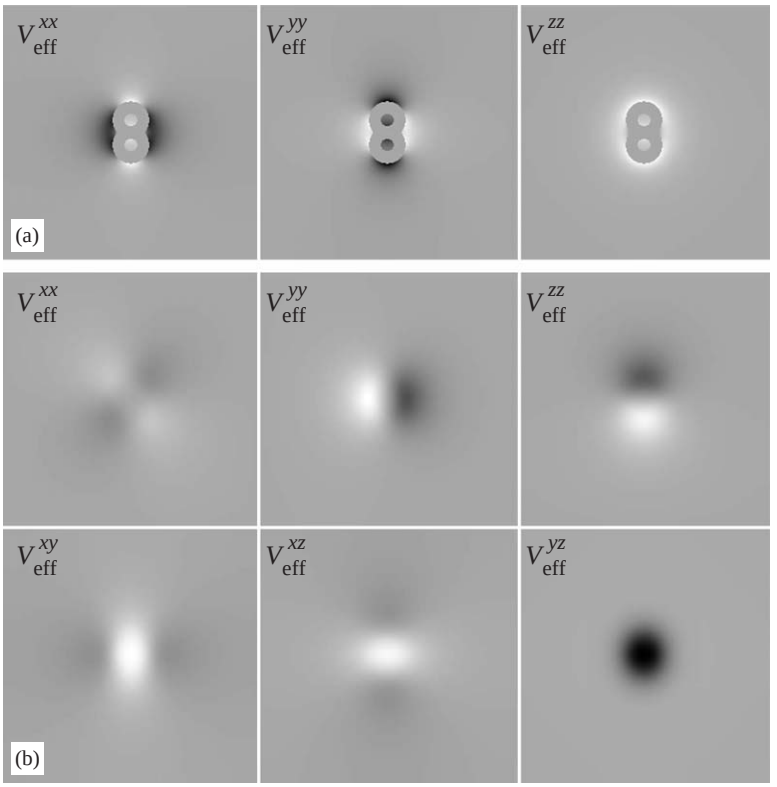

Fig. 4. Effective volume factors for the rings shown in Fig. 3: (a) depicts the diagonal components for $\boldsymbol{\rho}$ in the $(x, y, 0)$ plane. The intensities range from $-45\,\mathrm{nm}^3$ (black) to $+24\,\mathrm{nm}^3$ (white). The figure-eight corresponds to the vectors $\boldsymbol{\rho}$ for which the rings overlap. (b) Depicts all six tensor elements for the $(x, y, 32)$ plane, for which there is no possible overlap between the rings. The intensity range for this case is from $-18\,\mathrm{nm}^3$ (black) to $+9\,\mathrm{nm}^3$ (white).

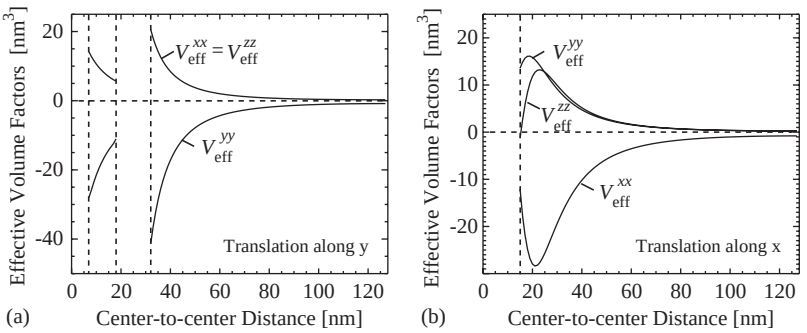

Fig. 5. Diagonal effective volume factors for the two rings as a function of translation distance along the y- (a) and x- (b) directions. The gaps in the curves correspond to translation values for which the rings overlap.

x-direction. The gaps in the curves correspond to an overlap of the two ring volumes. Such computations can be used as follows: consider the case where the center of the second ring is located at the point $\boldsymbol{\rho} = (0, 12.5, 0)\,\mathrm{nm}$, i.e., inside the horizontal ring (this corresponds to the situation depicted in Fig. 3). The effective volume factors (in nm^3) for this geometry (computed

numerically) are equal to:

$$V_{\mathrm{eff}}^{\alpha\beta} = \begin{pmatrix} 8.963 & 0.0 & 0.0 \\ 0.0 & -17.98 & 0.0 \\ 0.0 & 0.0 & 8.963 \end{pmatrix}. \tag{29}$$

The tensor is diagonal, and the diagonal elements are proportional to $(1, -2, 1)$, which is also the structure of the dipolar tensor for this particular choice of displacement $\boldsymbol{\rho}$. Therefore, similarly as for two dipoles, the minimum energy is reached when the magnetizations are aligned with respect to each other and with the displacement vector: $\hat{\mathbf{m}}_1 \| \hat{\mathbf{m}}_2 \| \pm \hat{\boldsymbol{\rho}}$. However, the exact value of the energy when the ring magnetizations are aligned in this fashion is a factor of 20 smaller than the energy computed from the pure dipole model. This is not surprising, given the close proximity and the complex geometry of the interlocking rings. The comparison between rings and dipoles has been made by considering two dipoles located at the same relative position $\boldsymbol{\rho}$, having the same total magnetic moment $\boldsymbol{\mu} = M_0 V \hat{\mathbf{m}}$ as the rings and substituting $\mathscr{D}$ in place of $\mathscr{N}$ in Eq. (10).

If the second ring center is located at the point $\boldsymbol{\rho} = (20, 20, 32)\,\mathrm{nm}$, then the effective volume tensor is non-diagonal, and not simply proportional to the dipolar tensor. This has an effect in establishing both the value and the location of the minimum energy state. For this geometry, the tensor is

$$V_{\mathrm{eff}}^{\alpha\beta} = \begin{pmatrix} 1.753 & -2.738 & -5.539 \\ -2.738 & 2.039 & -4.653 \\ -5.539 & -4.653 & -3.792 \end{pmatrix}.$$

Searching numerically for the minimum energy state, allowing the magnetizations to orient freely in 3D, we obtain that the two magnetizations are still aligned along a direction which, however, differs from $\hat{\boldsymbol{\rho}}$ by roughly 3°. The ring–ring energy is, in this case, just 4% smaller than the dipole–dipole. Restricting the search to in-plane magnetizations is, however, a more physical situation. In fact, the demagnetization factor $\langle N \rangle^{zz}$ for a ring having the specified parameters ($R_2 = 15\,\mathrm{nm}$, $R_1 = 10\,\mathrm{nm}$, $t = 4\,\mathrm{nm}$) is 0.553, which is larger than $\frac{1}{3}$. This implies that the magnetization will most likely be confined in the ring plane (see Ref. [16]). A 2D in-plane search for a minimum reveals that $\hat{\mathbf{m}}_1$ forms an angle of 36.5° with the x-axis, and $\hat{\mathbf{m}}_2$ is at 7.80° with the z-axis. By comparison, the same search for dipoles would result in a different pair of angles: 40.0° and 10.9°, with an associated 3% larger energy.

5. Conclusions

In this Letter, we have presented a novel theoretical and numerical approach to the computation of the magnetostatic pair interaction energy for uniformly magnetized shapes. A compact expression has been derived for a general shape–shape interaction, where the energy is computed by contracting a newly introduced magnetometric tensor field $\mathscr{N}$ with respect to the magnetic moments of the two bodies. The magnetometric tensor field is defined as the convolution between the cross-correlation function of the two shapes, and the dipolar tensor field. We have given examples of cross-correlation functions for a few basic shapes, as well as a geometrical interpretation for the convolution product that results in the magnetometric tensor field. The tensor field $\mathscr{N}$, and its associated effective volume factors, were explicitly computed for two interacting spheres and cubes. For the spheres we verified that the $\mathscr{N}$ coincides with the dipolar tensor $\mathscr{D}$; for the cubes we re-obtained the expression for the cube–cube interaction, which is widely employed in micromagnetic simulations. Finally, we sketched a numerical algorithm for the computation of the effective volume factors, followed by an example where the interaction between interlaced magnetized rings has been investigated thoroughly. By comparing the ring–ring and the dipole–dipole interactions we have shown that shape effects can change the location of the ground magnetic state in the free-parameters space, and its associated energy.

The method presented in this Letter, provides a unified way to deal with magnetic shapes. Perhaps the most important aspect of the method is that it cleanly separates the shape information (in the form of the cross-correlation function) from the dipolar field. This separation allows for a straightforward numerical implementation by means of fast Fourier transforms.

Acknowledgements

The authors would like to acknowledge stimulating interactions with S. Tandon, J. Zhu, Y. Zhu, Y. Millev and G. Rowlands. Financial support was provided by the US Department of Energy, Basic Energy Sciences, under Contract numbers DE-FG02-01ER45893 and DE-AC02-98CH10886.

References

[1] A. Aharoni, Introduction to the Theory of Ferromagnetism, 2nd Edition, Oxford University Press, Oxford, 2000.
[2] P. Asselin, A.A. Thiele, On the field Lagrangians in micromagnetics, IEEE Trans. Magn. 22 (1986) 1876–1880.
[3] P. Rhodes, G. Rowlands, Demagnetizing energies of uniformly magnetized rectangular blocks, Proc. Leeds Philos. Lit. Soc. 6 (1954) 191–210.
[4] A.D. Liu, H.N. Bertram, Modeling the effect of interactions in granular magnetic films, J. Appl. Phys. 89 (2001) 2861–2867.
[5] H.K. Lee, T.C. Schulthess, G. Brown, D.P. Landau, K.D. Sorge, J.R. Thompson, Magnetic properties of Fe nanocubes with magnetostatic interactions, J. Appl. Phys. 93 (2003) 7047–7049.
[6] H.K. Lee, T.C. Schulthess, D.P. Landau, G. Brown, J.P. Pierce, Z. Gai, G.A. Farnan, J. Shen, Monte Carlo simulations of interacting magnetic nanoparticles, J. Appl. Phys. 91 (2002) 6926–6928.
[7] M. Beleggia, S. Tandon, Y. Zhu, M. De Graef, On the magnetostatic interactions between nanoparticles of arbitrary shape, J. Magn. Magn. Mater. 278 (2004) 270–284.
[8] X.H. Huang, M. Pardavi-Horvath, Local demagnetizing tensor calculation for arbitrary non-ellipsoidal bodies, IEEE Trans. Magn. 32 (1996) 4180–4182.
[9] M. Beleggia, M. De Graef, On the computation of the demagnetization tensor field for an arbitrary particle shape using a fourier space approach, J. Magn. Magn. Mater. 263 (2003) L1–L9.
[10] S. Tandon, M. Beleggia, Y. Zhu, M. De Graef, On the computation of the demagnetization tensor for uniformly magnetized particles of arbitrary shape, Part I: analytical approach, J. Magn. Magn. Mater. 271 (2004) 9–26.
[11] S. Tandon, M. Beleggia, Y. Zhu, M. De Graef, On the computation of the demagnetization tensor for uniformly magnetized particles of arbitrary shape, Part II: numerical approach, J. Magn. Magn. Mater. 271 (2004) 27–38.
[12] A.G. Khachaturian, Theory of Structural Transformations in Solids, Wiley, New York, 1983.
[13] R.N. Bracewell, The Fourier Transform and its Applications, 2nd Edition, McGraw-Hill International Editions, New York, 1986.
[14] M.E. Schabes, A. Aharoni, Magnetostatic interaction fields for a three-dimensional array of ferromagnetic cubes, IEEE Trans. Magn. 23 (1987) 3882–3888.
[15] A. Hubert, R. Schäfer, Magnetic Domains, Springer, Berlin, 2000.
[16] M. Beleggia, J.W. Lau, M.A. Schofield, Y. Zhu, S. Tandon, M. De Graef, Phase diagram for magnetic nano-rings, Phys. Rev. B 2004, in press.